# **Dalton** Transactions



#### COMMUNICATION

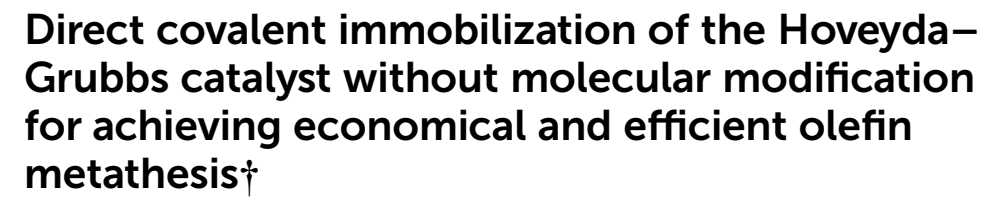
View Article Online



Cite this: Dalton Trans., 2025, 54. 12760

Received 19th June 2025, Accepted 23rd July 2025 DOI: 10.1039/d5dt01440a

rsc li/dalton



Chuangchuang He, Jincheng Duan, Yang Zhou, Junling Cui and Xuebing Ma 10 \*\*



The direct covalent immobilization of the Hoveyda-Grubbs catalyst into hollow mesoporous polystyrene nanospheres is developed via Friedel-Crafts alkylation without molecular modification for economical and efficient olefin metathesis.

Olefin metathesis reactions including ring-closing, cross-metathesis, acyclic diene polymerization, and ring-opening polymerization, catalysed by 1st and 2nd generation Hoveyda-Grubbs (HG) catalysts, are effective and powerful tools for the construction of carbon-carbon bonds, with broad applications in the synthesis of valuable pharmaceuticals,<sup>2</sup> fine chemicals,3 advanced polymers,4 and in the transformation of biomass into value-added chemicals.<sup>5</sup> Although homogeneous olefin metathesis offers obvious advantages in catalytic activity, the high cost of HG catalysts and their limited recoverability and reusability from reaction mixtures severely hinder their industrial-scale application. Currently, three main strategies have been developed to achieve the recovery and reuse of HG catalysts, involving encapsulation of HG catalysts in confined spaces, 6-10 homogeneous catalysis/two-phase separation, 11 and immobilization of HG catalysts onto solid supports.12 The encapsulation of HG catalysts into confined spaces enables the catalysts to promote reactions in a homogeneous-like manner, requiring no molecular modification. Unfortunately, precise control over the pore sizes of the confined spaces is extremely difficult and leads to loss of the HG catalyst. With respect to the unique advantages of homogeneous catalysis, several catalytic and two-phase separation systems, including tagged switchable-phase catalysts, <sup>13</sup> soluble polymer-supported catalysts,<sup>14</sup> light-controlled and pH-controlled phase strategies,<sup>15,16</sup> fluorous catalysts,<sup>17</sup> and nanofiltration, 18 have been developed to achieve homogeneous reactions in one phase followed by separation of HG catalysts in

modifications. The immobilization of homogeneous HG catalysts onto solid supports, which not only facilitates their separation from the reaction mixture but also realizes catalyst recycling, has become a promising strategy in both academic research and industrial applications. To date, many solid supports, such as silica-based, 19-40 polymer-based, 41-46 carbonbased, 47-50 and magnetic particle-based 51-53 materials, have been developed to achieve the recovery and reuse of catalysts after the completion of catalytic reactions. Nevertheless, timeand energy-consuming multi-step molecular modifications of HG catalysts are also required to install anchoring groups, such as silanization agents, 33-36 3-pyridyl bromide, 30,43 amides,<sup>37</sup> hydroxylates<sup>46</sup> and exchangeable ligands,<sup>22,26,44</sup> which enable HG catalysts to easily react with solid supports to achieve their effective immobilization (Scheme 1a). Therefore, it is highly desirable to develop a simple, convenient and general strategy for anchoring expensive HG catalysts onto catalyst supports to realize low-cost chemical synthesis. Inspired by the direct immobilization of expensive metal

another phase. However, to meet the demands of homo-

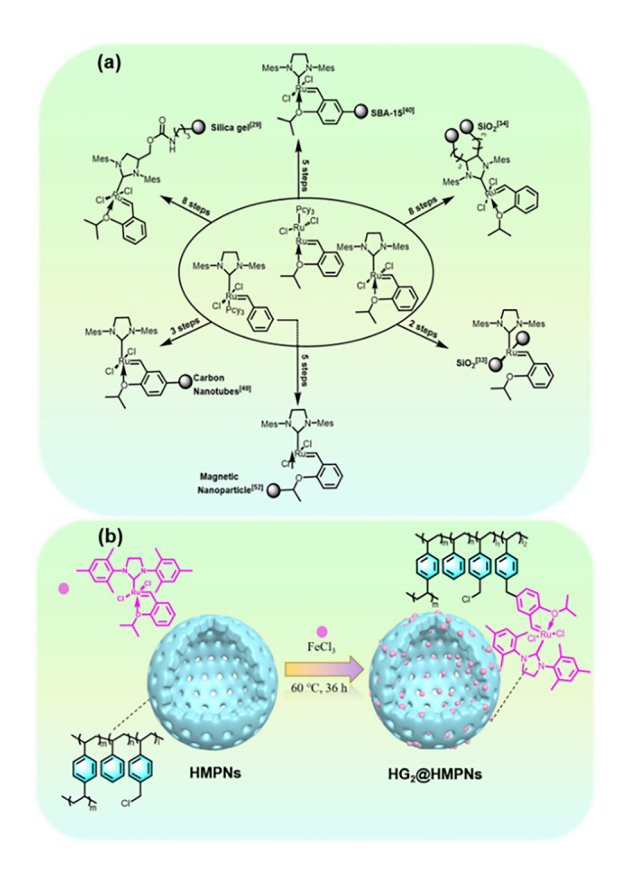
geneous catalysis, HG catalysts require multi-step molecular

complexes and chiral organocatalysts onto catalyst supports without molecular modification via Suzuki coupling, 54 Scholl reaction,<sup>55</sup> and Friedel-Crafts alkylation,<sup>56-60</sup> the present study applies Friedel-Crafts alkylation to immobilize the HG cata-(1,3-bis(2,4,6-trimethylphenyl)-2-imidazolidinylidene)lyst, dichloro(o-isopropylphenylmethylene) ruthenium directly onto hollow mesoporous polystyrene nanospheres (HMPNs) to fabricate an HMPN-supported (HG<sub>2</sub>@HMPNs) (Scheme 1b). Compared with previously reported multi-step immobilization strategies (Scheme 1a), this direct immobilization avoids multi-step molecular modification and effectively improves the utilization of the expensive HG2 catalyst. In particular, the as-prepared HG2@HMPNs possess a well-defined morphology with thin mesoporous shell and hollow interior, providing an ideal architectural structure for the reactants to rapidly access Ru catalytic sites. In the heterogeneous olefin metathesis of allylbenzoates and croto-

College of Chemistry and Chemical Engineering, Southwest University, Chongqing 400715, PR China, E-mail: zci123@swu.edu.cn

<sup>†</sup> Electronic supplementary information (ESI) available. See DOI: https://doi.org/ 10.1039/d5dt01440a

Dalton Transactions Communication



Scheme 1 (a) Synthetic routes for the covalent immobilization of expensive HG catalysts onto solid supports: multi-step molecular modification reported in previous works. (b) Direct covalent immobilization of HG<sub>2</sub> catalyst onto HMPNs described in the present work (b).

naldehyde,  $HG_2$ @HMPNs exhibit comparable catalytic yields to the homogeneous  $HG_2$  catalyst.

Owing to the electron-rich 2-isopropoxyphenyl moiety in the molecular structure of the HG $_2$  catalyst, the Friedel–Crafts alkylation occurs between HMPN-attached benzyl chloride ( $-C_6H_4CH_2Cl$ ) and 2-isopropoxyphenyl in the HG $_2$  catalyst. The conditions of the Friedel–Crafts alkylation including temperature, reaction time and the amount of FeCl $_3$  used are screened and the loading capacities of the HG $_2$  catalyst are shown in Table S1.† Under the optimal reaction conditions (60 °C, 36 h, 20 mol% FeCl $_3$ ), the highest loading capacity of HG $_2$  catalyst in HG $_2$ @HMPNs is determined by ICP-OES to be 0.46 mmol g $^{-1}$ .

The successful immobilization of the HG<sub>2</sub> catalyst onto the porous shell of HMPNs is confirmed by FT-IR, solid-state <sup>13</sup>C CP/MAS NMR and XPS spectra (Fig. 1). Compared with pristine HMPNs and free HG<sub>2</sub> catalyst, HG<sub>2</sub>@HMPNs exhibits FT-IR characteristic absorption signals of the HG<sub>2</sub> catalyst, including the stretching vibrations of Ru=CH at 2976 cm<sup>-1</sup> and C-O-C at 1251 cm<sup>-1</sup>, and the bending vibration of *i*-Pr at 1382 cm<sup>-1</sup> (Fig. 1a). Furthermore, in the <sup>13</sup>C CP/MAS NMR spectrum of HG<sub>2</sub>@HMPNs (Fig. 1b), signals corresponding to the HG<sub>2</sub> catalyst are observed, including Ru=CH at 288.3 ppm, NCHN at 153.8 ppm, phenyl groups in the range of 120–150 ppm, OCH at 77.1 ppm, and methyl and isopropyl carbons centered at

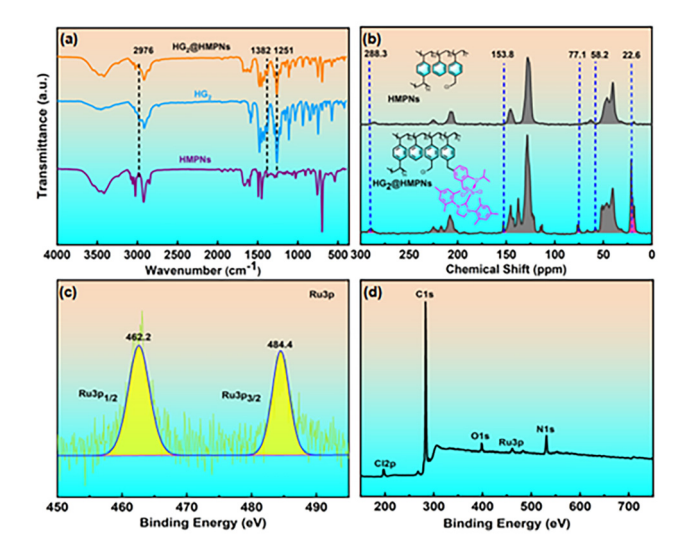


Fig. 1 (a) FT-IR of the  $HG_2$  catalyst, HMPNs and  $HG_2@HMPNs$ . (b) Solid-state  $^{13}C$  CP/MAS NMR spectra of HMPNs and  $HG_2@HMPNs$ . (c) The XPS spectrum of Ru 3p in  $HG_2@HMPNs$  and (d) the XPS spectrum of  $HG_2@HMPNs$ .

22.6 ppm. The intensity of the chloromethyl signal at 65.1 ppm is weakened, and a new peak at 58.2 ppm is assigned to a -CH2- linkage emerges, indicating reaction of -CH2Cl moieties of HMPNs and the electron-rich 2-isopropoxyphenyl group in the HG<sub>2</sub> catalyst. Additionally, the XPS spectra show the binding energies of all elements in HG<sub>2</sub>@HMPNs, including C 1s at 283.2 eV, O 1s at 398.7 eV, N 1s at 531.6 eV (Fig. 1d), Ru  $3p_{1/2}$  at 462.2 eV and Ru  $3p_{3/2}$  at 484.4 eV (Fig. 1c), respectively. The binding energy of Cl 2p at 199.5 eV indicates that some benzyl chloride moieties in HMPNs have not been completely consumed during the immobilization of the HG<sub>2</sub> catalyst (Fig. 1d), which is consistent with the result obtained from 13C CP/MAS NMR. Based on the above-mentioned results, it is confirmed that the HG2 catalyst is successfully anchored onto the porous shell of HMPNs via a -CH2linkage.

As observed from the SEM images (Fig. 2a and b), HG<sub>2</sub>@HMPNs retains the well-defined spherical morphology of their parent HMPNs, with particle size distribution of 224  $\pm$ 12 nm (n = 100) (Fig. 2i) compared to that of 201  $\pm$  12 nm for HMPNs (n = 100) (Fig. 2j). Owing to the pillaring effect of the anchored bulky HG<sub>2</sub> catalyst, the particle size of HG<sub>2</sub>@HMPNs is increased by about 23 nm. The TEM (Fig. 2e and f) and HAADF (Fig. 2c and d) images, clearly reveal a hollow interior is for both HMPNs and HG<sub>2</sub>@HMPNs. Furthermore, TEM-EDS elemental mappings of C and N atoms indicate that the HG<sub>2</sub> catalyst is evenly distributed on the porous shell of HG<sub>2</sub>@HMPNs (Fig. 2g and h). Upon anchoring of HG<sub>2</sub> onto HMPNs, the resultant HG<sub>2</sub>@HMPNs exhibit no significant change in the volume of adsorbed N2 (Fig. 2k). However, the pore size becomes narrow due to the space occupied by the anchored HG2 catalyst, and some smaller mesopores centered at 5.2 nm and 7.5 nm are newly constructed in the shell of

10

26

21

33

34

32

32

64

83

80

72

Communication **Dalton Transactions** 

Ethanol

Toluene

**DMSO** 

10

11

12

13

14

15

16

17

18

19

20

20

20

0

30

40

60

2.0

20

2.0

20

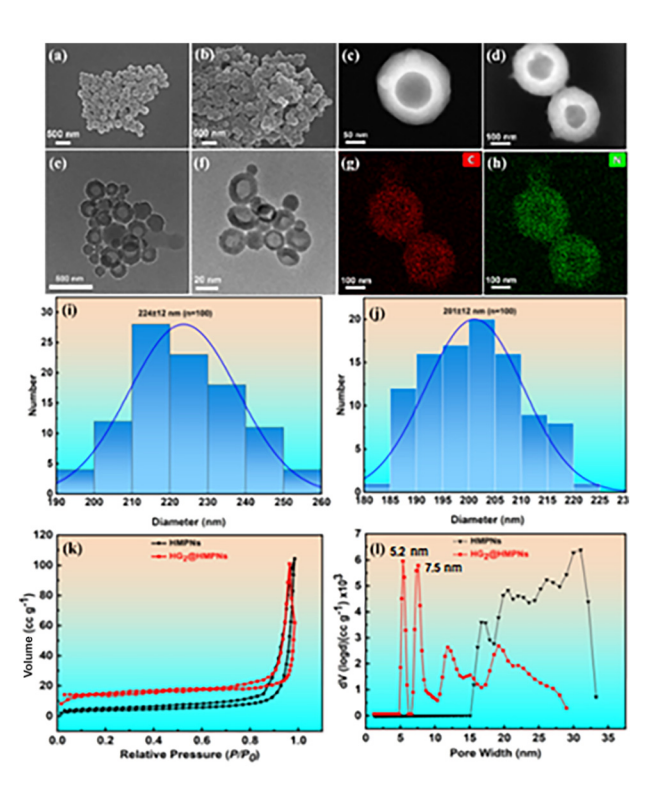


Fig. 2 SEM images of (a) HMPNs and (b) HG2@HMPNs. HAADF of (c) HMPNs and (d) HG<sub>2</sub>@HMPNs. TEM images of (e) HMPNs and (f) HG<sub>2</sub>@HMPNs. TEM-EDS mappings of (g) carbon and (h) nitrogen for HG<sub>2</sub>@HMPNs. Particle size distributions of (i) HG<sub>2</sub>@HMPNs and (j) HMPNs based on the SEM images. (k) N2 adsorption-desorption isotherms and (I) pore size distributions of HMPNs and HG<sub>2</sub>@HMPNs.

HG<sub>2</sub>@HMPNs (Fig. 21). Overall, the as-fabricated HG<sub>2</sub>@HMPNs possess spherical morphology similar to their parent HMPNs with a hollow interior and a thin and mesoporous shell, which facilitates fast mass transfer of reactants to the Ru catalytic sites during heterogeneous catalysis.<sup>61</sup>

The conditions of the HG2@HMPN-promoted heterogeneous olefin metathesis reaction between allylbenzoate and crotonaldehyde,62 including solvent, reaction temperature and the amount of catalyst used, were optimized and the details are shown in Table 1. When the amount of HG2 catalyst used in HG<sub>2</sub>@HMPNs is set to 1.0 mol%, the product is afforded at its highest yield (39%) in toluene at 20 °C during 30 min of reaction. This result is attributed to non-polar toluene being more suitable than other solvents for the generation of weakly polar intermediates in the catalytic cycle. Upon increasing or decreasing the reaction temperature, no better yield of product is obtained. When the amount of anchored HG2 catalyst is increased from 1.0 mol% to 5.0 mol%, the yield of product is significantly improved to 83%. However, subsequently doubling the dosage of HG2 catalyst to 10 mol% leads to a decreased yield (80%), likely due to reduced swellability of HG<sub>2</sub>@HMPNs in toluene (2 mL), resulting in narrower pore sizes that restrict access of reactants to the interior Ru catalytic sites.<sup>57</sup> Furthermore, no better yield is obtained by prolonging the reaction time to 40 min. It is concluded that the best yield

Table 1 Optimization of heterogeneous olefin metathesis reaction conditions<sup>a</sup>

HG<sub>2</sub>@HMPNs (x mol%)

|       |          |       | Solvent       |                |                        |   |
|-------|----------|-------|---------------|----------------|------------------------|---|
| Entry | Solvent  | Temp. | Time<br>(min) | Cat.<br>(mol%) | Yield <sup>b</sup> (%) | _ |
| 1     | Toluene  | 20    | 30            | 1.0            | 39                     | _ |
| 2     | DCM      | 20    | 30            | 1.0            | 28                     |   |
| 3     | DCE      | 20    | 30            | 1.0            | 36                     |   |
| 4     | THF      | 20    | 30            | 1.0            | 30                     |   |
| 5     | $CHCl_3$ | 20    | 30            | 1.0            | 33                     |   |
| 6     | DMF      | 20    | 30            | 1.0            | 20                     |   |
| 7     | Acetone  | 20    | 30            | 1.0            | 25                     |   |
| 8     | Methanol | 20    | 30            | 1.0            | 15                     |   |
|       |          |       |               |                |                        |   |

30

30

30

30

30

30

30

30

30

30

2.0

40

1.0

1.0

1.0

1.0

1.0

1.0

1.0

3.0

5.0

10.0

5.0

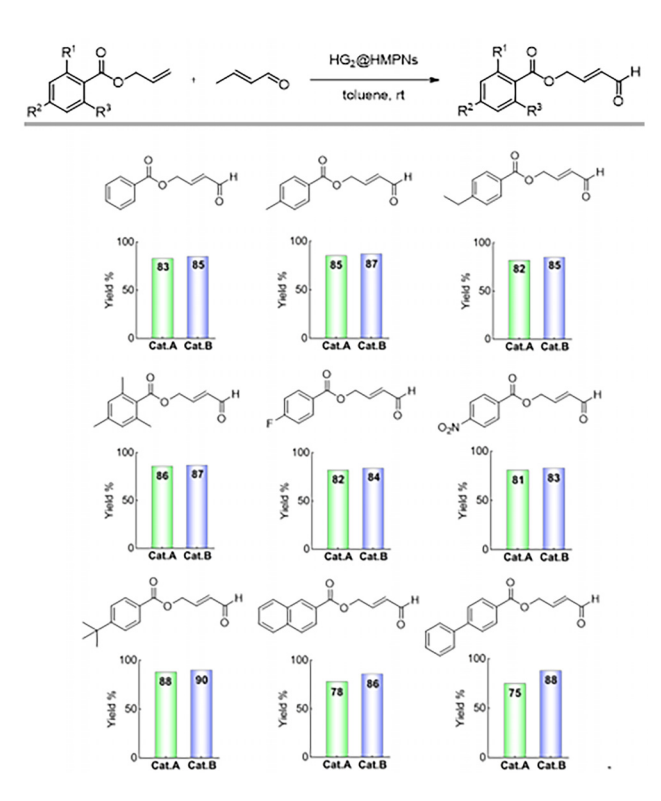
5.0

(83%) is obtained during heterogeneous catalysis using HG<sub>2</sub>@HMPNs under the following optimal conditions: toluene (2 mL), 5.0 mol% of HG2 catalyst in HG2@HMPNs (108.0 mg), substrates (1.0 mmol), 20 °C, 30 min. In particular, the selfmetathesis of allylbenzoate has also been confirmed,62 while crotonaldehyde is not fully consumed under the optimized conditions.

Under the optimal reaction conditions, the substrate scope was expanded to various allylbenzoates to further evaluate the catalytic activity of HG2@HMPNs (Scheme 2). Whatever the electron-donating ( $R^1 = CH_3$ ,  $CH_2CH_3$ , t-Bu) or electron-withdrawing substituent groups  $(R_1 = F, NO_2)$  that are attached to the phenyl ring of the allylbenzoates, HG<sub>2</sub>@HMPNs affords good product yields (81-88%) comparable to those when using the homogeneous  $HG_2$  catalyst (83–90%). The reduction in yield of less than 3% suggests that the characteristic morphology of HG<sub>2</sub>@HMPNs with their hollow interior and mesoporous and swellable shell facilitates efficient mass transfer of reactants to the Ru catalytic sites, even under heterogeneous conditions. Unfortunately, HG2@HMPNs promote the reactions of bulky allyl naphthalate and allylbenzoate ( $R_2 = Ph$ ) with crotonaldehyde to afford the corresponding products in significantly lower yields. Compared with the homogeneous HG2 catalyst, HG2@HMPNs afford the corresponding products with yield reductions of 8% and 13%, respectively. The reason for this is attributed to limited mass transfer within the porous channels of HG<sub>2</sub>@HMPNs, where bulky allylbenzoates bearing naphthyl and biphenyl moieties encounter steric hin-

<sup>&</sup>lt;sup>a</sup> Reaction conditions: allylbenzoate (162.2 mg, 1.0 mmol), crotonaldehyde (70.1 mg, 1.0 mmol), HG<sub>2</sub>@HMPNs, solvent (2 mL), 30 min. Isolated yields.

**Dalton Transactions** Communication



Scheme 2 Olefin metathesis of various allylbenzoates with crotonaldehyde catalysed by HG2@HMPNs (Cat. A) and homogeneous HG2 catalyst (Cat. B). Reaction conditions: allylbenzoates (1.0 mmol), crotonaldehyde (70.1 mg, 1.0 mmol), toluene (2 mL), HG<sub>2</sub>@HMPNs (108.0 mg, 5.0 mol% of HG<sub>2</sub> catalyst), 20 °C, 30 min.

drance from the pore walls, leading to limited access to interior Ru catalytic sites. To improve the reactivity of bulky allylbenzoates, the amount of cross-linking agent (DVB) used in the preparation of HMPNs was reduced by 20%. The obtained HG2@HMPNs with their enhanced swellability affords products at significantly improved yields of 84% and 81%, respectively, due to the larger pore sizes of HMPNs in organic solvent. Unfortunately, a further decrease, where the amount of DVB was reduced by 40% causes HMPNs to lose their well-defined spherical morphology. Moreover, in comparison with homogeneous catalysis, there is no change in the E/Z outcomes of products.

Following completion of the olefin metathesis of 2,4,6-trimethylbenzoate and crotonaldehyde, HG2@HMPNs can be easily recovered via centrifugation, washed with ethyl acetate, dried naturally, and reused directly in subsequent catalytic cycles. As shown in Fig. 3a, gram-scale heterogeneous olefin metatheses show no significant decrease in yield during eight cycles of using HG<sub>2</sub>@HMPNs. The morphology, Ru content and porous structure of the 8th-reused HG2@HMPNs were characterized by SEM, ICP-OES and N2 adsorption-desorption isotherms. It can be seen from the SEM image that the 8<sup>th</sup>reused HG<sub>2</sub>@HMPNs maintain the well-defined spherical morphology observed in the freshly made HG<sub>2</sub>@HMPNs (Fig. 3b), indicating that HG<sub>2</sub>@HMPNs possess good mechanical stabi-

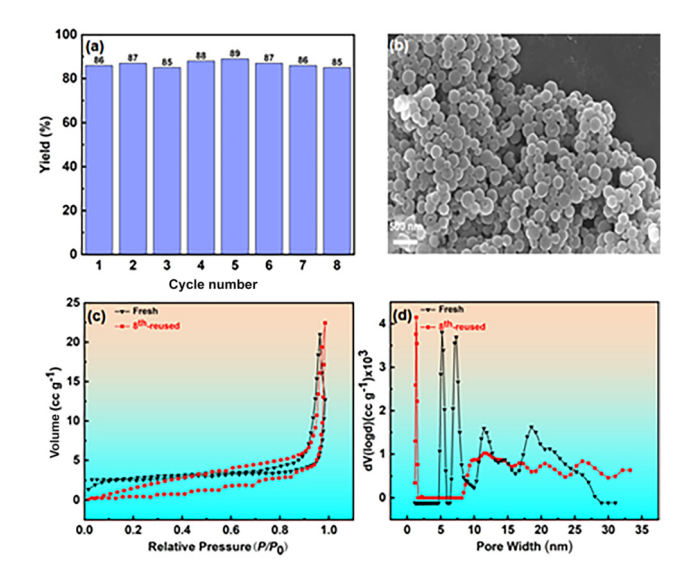


Fig. 3 (a) Yields of product following the reuse of HG<sub>2</sub>@HMPNs during the olefin metathesis of allylbenzoate and crotonaldehyde under the following conditions: 2.4.6-trimethylbenzoate (1.02 g. 5.0 mmol), crotonaldehyde (0.35 g, 5.0 mmol), toluene (10 mL), HG<sub>2</sub>@HMPNs (0.54 g, 5.0 mol% Ru), 20 °C, 30 min. (b) SEM image of the 8<sup>th</sup>-reused HG<sub>2</sub>@HMPNs. (c) N<sub>2</sub> adsorption-desorption isotherms and (d) pore size distributions of the pristine and 8<sup>th</sup>-reused HG<sub>2</sub>@HMPNs.

lity. Furthermore, the Ru content in the 8<sup>th</sup>-reused HG<sub>2</sub>@HMPNs, as determined by ICP-OES, was found to be 0.44 mmol g<sup>-1</sup>, revealing that the covalently anchored HG<sub>2</sub> catalyst exhibits good chemical stability during repeated catalytic processes. Notably, the Ru concentration in the corresponding reaction mixtures remained in the range of 0.008-0.012‰ during the catalytic cycles, as measured by ICP-OES. Following purification of the reaction residue by column chromatography, no detectable ruthenium was found in the isolated pure products. Moreover, the N2 adsorption-desorption isotherms reveal no obvious change in the total adsorbed volume of N2 (Fig. 3c). In contrast, the pore size distribution of the 8<sup>th</sup>-reused HG<sub>2</sub>@HMPNs differs greatly in comparison with that of the pristine sample. The mesopores originally centered at 5.2 nm and 7.5 nm disappear, while new micropores centered at 1.3 nm have emerged, possibly resulting from the accumulation of reactants and/or products within these pores. Owing to the maintenance of the mesopores above 8 nm, the mass transfer of reactants is not significantly affected. Therefore, it is considered that the blockage of the mesopores by reactants and/or products and the negligible loss of anchored Ru catalyst are responsible for the small decreases in yield during the reuse of HG<sub>2</sub>@HMPNs.

In this communication, the HG<sub>2</sub> catalyst is directly immobilized onto HMPNs via Friedel-Crafts alkylation, without prior molecular modification. This strategy avoids the previously reported multi-step molecular modification of the catalyst, effectively improving the utilization of the HG2 catalyst. The as-fabricated HMPN-supported HG2 catalyst possesses a hollow interior and a thin, mesopore-abundant shell, providCommunication **Dalton Transactions** 

ing an architecture ideally suited to the fast mass transfer of reactants to facilitate access to Ru catalytic sites. In the heterogeneous olefin metathesis of allylbenzoates and crotonaldehyde, comparable yields to homogeneous counterparts and good reusability of the catalyst can be achieved. Overall, this direct immobilization of the HG2 catalyst onto HMPNs via Friedel-Crafts alkylation provides a reference for the immobilization of other expensive HG catalysts, achieving the low-cost synthesis of fine chemicals.

#### **Author contributions**

Chuangchuang He: Investigation, visualization, methodology, formal analysis, validation, and writing - original draft; Jincheng Duan: Investigation; Yang Zhou: Investigation; Junling Cui: Investigation; Xuebing Ma: Conceptualization, funding acquisition, project administration, methodology, and writing - review & editing.

#### Conflicts of interest

There are no conflicts to declare.

### Data availability

The data supporting this article have been included as part of the ESI.†

## Acknowledgements

This work was financially supported by the National Natural Science Foundation of China (51973177).

#### References

- 1 O. M. Ogba, N. C. Warner, D. J. O'Leary and R. H. Grubbs, Chem. Soc. Rev., 2018, 47, 4510-4544.
- 2 D. F. Sauer, J. Schiffels, T. Hayashi, U. Schwaneberg and J. Okuda, Beilstein J. Org. Chem., 2018, 14, 2861-2871.
- 3 M. Jeschek, S. Panke and T. R. Ward, Trends Biotechnol., 2018, 36, 60-72.
- 4 G. I. Peterson, S. Yang and T. L. Choi, Acc. Chem. Res., 2019, 52, 994-1005.
- 5 T. Tiso, D. F. Sauer, K. Beckerle, C. C. Blesken, J. Okuda and L. M. Blank, Catalysts, 2020, 10, 874.
- 6 H. Yang, Z. Ma, T. Zhou, W. Zhang, J. Chao and Y. Qin, ChemCatChem, 2013, 5, 2278-2287.
- 7 M. Aşkun, K. Sagdic, F. Inci and B. Ö. Öztürk, Catal. Sci. Technol., 2022, 12, 6174-6183.
- 8 Z. Tunalı, K. Sagdic, F. Inci and B. Ö. Öztürk, React. Chem. Eng., 2022, 7, 1617-1625.
- 9 Q. Li, T. Zhou and H. Yang, ACS Catal., 2015, 5, 2225–2231.

- 10 B. Ö. Öztürk, A. Hillik, B. N. Kücük and F. Inci, Dalton Trans., 2025, 54, 8658.
- 11 M. Al-Hashimi, R. Tuba, H. S. Bazzi and R. H. Grubbs, ChemCatChem, 2015, 8, 228-233.
- 12 M. O. Lvanytsya, S. V. Ryabukhin, D. M. Volochnyuk and S. V. Kolotilov, Theor. Exp. Chem., 2020, 56, 283-308.
- 13 R. Duque, E. Öchsner, H. Clavier, F. Caijo, S. P. Nolan, M. Mauduit and D. J. C. Hamilton, Green Chem., 2011, 13, 1187-1195.
- 14 M. Al-Hashimi, R. Tuba, H. S. Bazzi and R. H. Grubbs, ChemCatChem, 2015, 8, 228-233.
- 15 G. Liu and J. Wang, Angew. Chem., Int. Ed., 2010, 49, 4425-
- 16 Y. Duan, T. Wang, Q. Xie, X. Yu, W. Guo, S. Wu, D. Li, J. Wang and G. Liu, Dalton Trans., 2017, 46, 5986-5993.
- 17 M. Matsugi and D. P. Curran, J. Org. Chem., 2005, 70, 1636-
- 18 D. Schoeps, K. Buhr, M. Dijkstra, K. Ebert and H. Plenio, Chem. - Eur. J., 2009, 15, 2960-2965.
- 19 J. Pastva, K. Skowerski, S. J. Czarnocki, N. Žilková, J. Čejka, Z. Bastl and H. Balcar, ACS Catal., 2014, 4, 3227-3236.
- 20 E. Borré, M. Rouen, I. Laurent, M. Magrez, F. Caijo, C. Crévisy, W. Solodenko, L. Toupet, R. Frankfurter, C. Vogt, A. Kirschning and M. Mauduit, Chem. - Eur. J., 2012, 18, 16369-16382.
- 21 N. J. M. Pijnenburg, E. Tomás-Mendivil, K. E. Mayland, H. Kleijn, M. Lutz, A. L. Spek, G. van Koten and R. J. M. K. Gebbink, Inorg. Chim. Acta, 2014, 409, 163-173.
- 22 J. L. Cheong, D. Wong, S. G. Lee, J. Lim and S. S. Lee, Chem. Commun., 2015, 51, 1042-1045.
- 23 H. Balcar, N. Žilková, M. Kubů, M. Polášek and J. Zedník, Catal. Today, 2018, 304, 127-134.
- 24 B. Werghi, E. Pump, M. Tretiakov, E. A. Hamad, A. Gurinov, P. Doggali, D. H. Anjum, L. Cavallo, A. Bendjeriou-Sedjerari and J. M. Basset, Chem. Sci., 2018, 9, 3531-3537.
- 25 P. D. Nieres, V. A. Vaillard, J. Zelín, N. I. Neuman, A. F. Trasarti, C. R. Apesteguía and S. E. Vaillard, ChemCatChem, 2023, 15, e202300010.
- 26 J. Lim, S. S. Lee, S. N. Riduan and J. Y. Ying, Adv. Synth. Catal., 2007, 349, 1066-1076.
- 27 J. Lim, S. S. Lee and J. Y. Ying, Chem. Commun., 2010, 46, 806-808.
- 28 H. Yang, Z. Ma, Y. Wang, Y. Wang and L. Fang, Chem. Commun., 2010, 46, 8659-8661.
- 29 D. P. Allen, M. M. Van Wingerden and R. H. Grubbs, Org. Lett., 2009, 11, 1261-1264.
- 30 J. Cabrera, R. Padilla, M. Bru, R. Lindner, T. Kageyama, K. Wilckens, S. L. Balof, H. J. Schanz, R. Dehn, J. H. Teles, S. Deuerlein, K. Müller, F. Rominger and M. Limbach, Chem. - Eur. J., 2012, 18, 14717-14724.
- 31 M. P. Conley, C. Copéret and C. Thieuleux, ACS Catal., 2014, 4, 1458-1469.
- 32 C. del Pozo, A. Corma, M. Iglesias and F. Sánchez, J. Catal., 2012, 291, 110-116.

Dalton Transactions Communication

- 33 B. Marciniec, S. Rogalski, M. J. Potrzebowski and C. Pietraszuk, *ChemCatChem*, 2011, 3, 904–910.
- 34 A. Monge-Marcet, R. Pleixats, X. Cattoën and M. W. C. Man, *J. Mol. Catal. A:Chem.*, 2012, 357, 59–66.
- 35 A. M. Marcet, R. Pleixats, X. Cattoën and M. W. C. Man, *Tetrahedron*, 2013, **69**, 341–348.
- 36 H. Nasrallah, A. Pagnoux, D. Didier, C. Magnier, L. Toupet, R. Guillot, C. Crévisy, M. Mauduit and E. Schulz, Eur. J. Org. Chem., 2014, 7781–7787.
- 37 H. Nasrallah, D. Dragoe, C. Magnier, C. Crévisy, M. Mauduit and E. Schulz, *ChemCatChem*, 2015, 7, 2493– 2500.
- 38 M. K. Samantaray, J. Alauzun, D. Gajan, S. Kavitake, A. Mehdi, L. Veyre, M. Lelli, A. Lesage, L. Emsley, C. Copéret and C. Thieuleux, J. Am. Chem. Soc., 2013, 135, 3193–3199.
- 39 B. Van Berlo, K. Houthoofd, B. F. Sels and P. A. Jacobs, *Adv. Synth. Catal.*, 2008, **350**, 1949–1953.
- 40 H. Zhang, Y. Li, S. Shao, H. Wu and P. Wu, *J. Mol. Catal. A: Chem.*, 2013, 372, 35–43.
- 41 S. W. Chen, J. H. Kim, C. E. Song and S. G. Lee, *Org. Lett.*, 2007, **9**, 3845–3848.
- 42 C. Hongfa, H.-L. Su, H. S. Bazzi and D. E. Bergbreiter, *Org. Lett.*, 2009, **11**, 665–667.
- 43 A. Kirschning, K. Mennecke, K. Grela and U. Kunz, *Synlett*, 2005, **19**, 2948–2952.
- 44 Q. Yao and Y. Zhang, J. Am. Chem. Soc., 2004, 126, 74-75.
- 45 C. Hobbs, Y. C. Yang, J. Ling, S. Nicola, H. L. Su, H. S. Bazzi and D. E. Bergbreiter, *Org. Lett.*, 2011, 13, 3904–3907.
- 46 L. Xia, T. Peng, G. Wang, X. Wen, S. Zhang and L. Wang, *ChemistryOpen*, 2019, **8**, 45–48.

- 47 D. V. Espinosa, C. Vicent, M. Baya and J. A. Mata, *Catal. Sci. Technol.*, 2016, 6, 8024–8035.
- 48 S. Lee, J. Y. Shin and S. g. Lee, *Chem. Asian J.*, 2013, 8, 1990–1993.
- 49 G. Liu, B. Wu, J. Zhang, X. Wang, M. Shao and J. Wang, Inorg. Chem., 2009, 48, 2383–2390.
- 50 S. Sabater, J. A. Mata and E. Peris, ACS Catal., 2014, 4, 2038–2047.
- 51 B. Ö. Öztürk, Microporous Mesoporous Mater., 2018, 267, 249–256.
- 52 S. W. Chen, Z. C. Zhang, M. Ma, C. M. Zhong and S. g. Lee, *Org. Lett.*, 2014, **16**, 4969–4971.
- 53 Y. H. Zhu, L. Kuijin, N. Huimin, C. Z. Li, L. P. Stubbs, C. F. Siong, T. Muihua and S. C. Peng, *Adv. Synth. Catal.*, 2009, 351, 2650–2656.
- 54 C. C. He, J. P. Duan and X. B. Ma, *Mol. Catal.*, 2024, **567**, 114480.
- 55 J. N. Zhang and X. B. Ma, Appl. Catal., A, 2024, 675, 119633.
- 56 M. Y. Xie, W. Y. Tian and X. B. Ma, Appl. Catal., A, 2024, 684, 119905.
- 57 J. Liu, H. Zhu, J. N. Zhang, W. Y. Tian and X. B. Ma, J. Catal., 2023, 425, 322–332.
- 58 W. Y. Tian, Y. Y. Luo, S. W. Zhu, Y. Zhou, C. C. He and X. B. Ma, *Dalton Trans.*, 2025, **54**, 8055–8060.
- 59 J. N. Zhang, S. Li, J. Liu and X. B. Ma, Appl. Catal., A, 2023, 649, 118976.
- 60 S. Li, J. N. Zhang, S. Q. Chen and X. B. Ma, J. Catal., 2022, 416, 139–148.
- 61 G. X. Xie, S. Wei, L. Zhang and X. B. Ma, *Ind. Eng. Chem. Res.*, 2019, **58**, 2812–2823.
- 62 R. L. Pederson, I. M. Fellows, T. A. Ung, H. Ishihara and S. P. Hajela, *Adv. Synth. Catal.*, 2002, **344**, 728–735.